SEPARATED FLOW AROUND A FLAT PLATE AT HIGH INCIDENCE: AN LES INVESTIGATION

Michael Breuer and Nikola Jovičić
Institute of Fluid Mechanics, University of Erlangen–Nürnberg
D–91058 Erlangen, Germany
breuer@lstm.uni-erlangen.de
njovicic@lstm.uni-erlangen.de

ABSTRACT

The separated flow past an inclined, nominally two–dimensional flat plate was investigated based on large eddy simulation. The configuration chosen ($Re_c = 20,000, \alpha = 18°$) is similar to a corresponding experimental investigation for airfoils at high angle of attack which is the final objective. In order to assure reliable results in a preliminary study the influence of the spanwise extension and the corresponding resolution was examined carefully leading to the final configuration. The flow field around a flat plate in this range of inclination is dominated by an asymmetric vortex shedding cycle with a Strouhal number $St' \approx 0.2$. A strong vortex develops almost periodically in the vicinity of the trailing edge. The life cycle of this vortex structure is controlling the entire flow field. At the leeward side of the plate a large clockwise rotating recirculation region of nearly constant pressure exists. A periodically occurring shedding motion of these vortical structures into the wake is not observed.

INTRODUCTION

The objective of the present investigation is to study incompressible turbulent flows with large separation regions based on large eddy simulation (LES). Flows of this type occur in many aerodynamic applications such as airfoils at high–lift conditions. Because most RANS models fail to predict this flow reasonable, some national/international projects have been initiated to investigate the feasibility of LES for high–lift airfoil flows at high Reynolds numbers. One of these is the European project LESFOIL (Davidson, 2000), in which the flow around an Aerospatiale A–airfoil is studied at an angle of attack $\alpha = 13.3°$ and a chord Reynolds number $Re_c = u_\infty c/\nu = 2.1 \cdot 10^6$.

In order to study the physics of stalled airfoil flows in detail, the present work aims at a slightly different configuration experimentally investigated within the COSTWING experiment by Lerche and Dallmann (1999). A nominally 2D airfoil based on a NACA–4415 profile is mounted inside a channel ($Re_c = 8 \cdot 10^4 - 10^6, \alpha = 0°$ and 22.5°). However, before starting with the NACA–4415 airfoil case, the flow around the simplest high–lift configuration was investigated, namely an inclined, infinitely thin flat plate ($\alpha = 18°$). In order to ensure a reasonable resolution and therefore reliable results, the present study was restricted to $Re_c = 20,000$. The flow separates at the sharp edge leading to a shear layer where transition takes place. On the leeward side of the plate a large recirculation region exists. Furthermore, at the trailing edge a second shear layer generates vortical structures of high intensities. Both processes together are forming an asymmetric von Kármán vortex street behind the plate. Therefore, large vortical structures and recirculation regions are dominating the flow recommending LES as an appropriate tool for the investigation.

NUMERICAL METHODOLOGY

The LES code $\mathcal{LESOCC}$ used for the solution of the filtered Navier–Stokes equations, is based on a 3–D finite–volume method for arbitrary non–orthogonal and non–staggered (block–structured) grids (Breuer and Rodi, 1996; Breuer, 1998, 2000). The spatial discretization of all fluxes is based on central differences of second–order accuracy. A low–storage multi–stage Runge–Kutta method (second–order accurate) is applied for time–marching. In order to ensure the coupling of pressure and velocity fields on non–staggered grids, the momentum interpolation technique is used. For modeling the non–resolvable subgrid scales (SGS), two different models are implemented, namely the well–known Smagorin-

sky model with Van Driest damping near solid walls and the dynamic approach with a Smagorinsky base model. Owing to the low Reynolds number of this investigation, the influence of the SGS model is expected to be small. Therefore, only the Smagorinsky model with a standard constant of $C_s = 0.1$ is applied. The code and the implemented SGS models were validated on a variety of different test cases, see, e.g. (Breuer and Rodi, 1996; Breuer, 1998, 2000; Rodi *et al.*, 1997). $\mathcal{LESOCC}$ is highly vectorized and additionally parallelized by domain decomposition with explicit message–passing based on MPI allowing efficient computations especially on vector–parallel machines. The present simulations were carried out on the Hitachi SR 8000–F1 applying 8 nodes (= 8 × 8 processors).

DESCRIPTION OF THE CONFIGURATION

Fig. 1 shows the configuration of the flow around the inclined flat plate. At the $Re_c = 20,000$ used in this simulation, no–slip boundary conditions can be applied at the surface of the flat plate. To save grid points the boundary layers of the channel walls (see Fig. 1) are not resolved and approximated by slip–conditions. Owing to the channel configuration of COST-WING a lot of grid points can be saved because the far–field does not have to be resolved. To further simplify numerical simulations, the experiment was especially designed in such a way that either statistically two–dimensional or spanwise periodical flow structures can be expected. Therefore in the present LES, periodicity in the spanwise direction is assumed. At the inlet a constant velocity u_∞ is prescribed, whereas at the outlet a convective boundary condition assures that vortices can pass through the outflow boundary. In order to investigate the effect of the spanwise extension/resolution four simulations with different domain sizes and spanwise resolutions were performed. More detailed information about the grids used for these simulations is given in Table 1.

	no. of blocks	no. of grid points/block	total no. of points	domain size in z–direction
2D	8	150 × 100	$1.2 \cdot 10^5$	–
I	8	150 × 100 × 48	$5.76 \cdot 10^6$	$0.1 \times c$
II	8	150 × 100 × 48	$5.76 \cdot 10^6$	$1.0 \times c$
III	8	150 × 100 × 72	$8.64 \cdot 10^6$	$1.0 \times c$

Table 1: Summary of the grid information for the performed simulations.

In Fig. 2 a x–y plot of one of these grids is depicted exemplarily, whereupon only every fifth grid line is shown. The grid points are clustered in the vicinity of the thin plate and towards the leading and trailing edges, so that the grid spacing in these regions is approximately $0.001 \times c$ in wall normal and in flow direction.

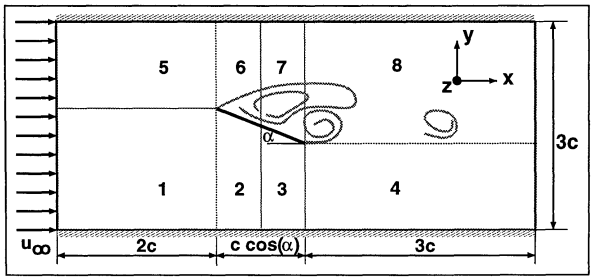

Figure 1: Two–dimensional sketch of the geometry including multi–block boundaries.

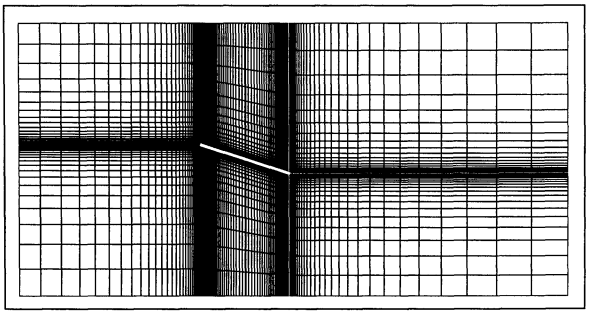

Figure 2: x-y plane of the computational grid, only every fifth grid line is shown.

RESULTS AND DISCUSSION

Investigation of Spanwise Extension and Resolution

The use of an adequate domain size and resolution in spanwise direction is of major importance in order to obtain reliable and physically reasonable results for such kind of flows. Therefore, the two–point correlations in spanwise direction of all velocity fluctuations (u', v', w') were evaluated. This was done for the simulations I and II at two different locations above the flat plate. As a result the two–point correlations of simulation I did not vanish in half width of the domain size chosen and therefore showed the insufficiency of the spanwise extension of $0.1 \times c$. In contrast the correlations for simulation II point to an adequately chosen domain size in spanwise direction. Admittedly for the latter case the resolution in this direction is ten times coarser than for the former simulation since the number of grid points was retained. However, the results of simulation III with a slightly improved resolution in z–direction yielded not much of a difference with regard to simulation II. Further grid re-

finement in spanwise direction would have led to an increased problem size and simulation time and was not considered necessary anyway. Therefore, the final configuration is a well–balanced compromise between spanwise extension and spanwise resolution. This is reflected by the results discussed in the following section.

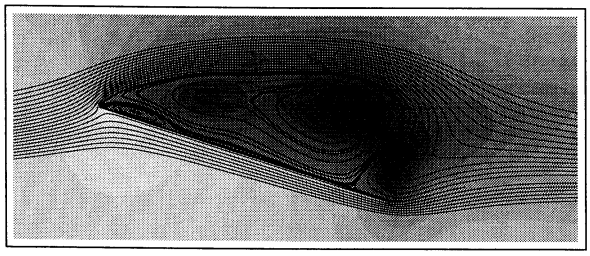

Figure 3: Time–averaged flow field, streamlines and pressure field, Simulation 2D.

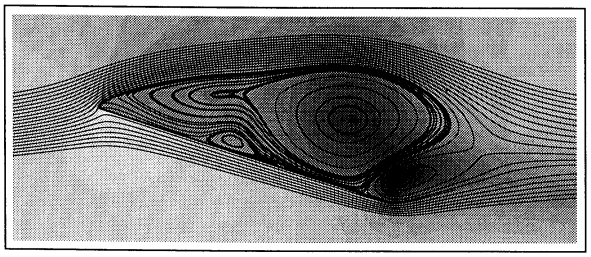

Figure 4: Time–averaged flow field, streamlines and pressure field, Simulation I.

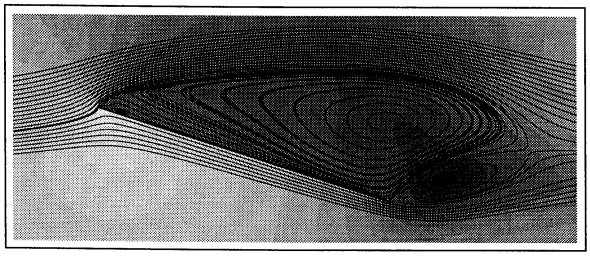

Figure 5: Time–averaged flow field, streamlines and pressure field, Simulation III.

In Figs. 3–5 the time–averaged flow field of the simulations 2D, I and III, respectively, are shown by pressure contours and streamlines. The flow field of simulation II is omitted since it does not differ significantly from simulation III. As expected, the flow separates at the leading edge and forms a large clockwise rotating recirculation region on the leeward side of the plate in all cases. However, there is a major difference concerning the flow around the trailing edge of the plate. Whereas the trailing edge vortex in the simulations 2D and I resides upon the end of the plate, in simulation III this vortex is shifted behind the plate (see also Figs. 7 and 8). This circumstance is attributed directly to the insufficient spanwise extension of the domain used in simulation I, respectively to the incapability of a two–dimensional simulation for such flows with large separation regions and the Reynolds number chosen. The differences in the location of the trailing edge vortex for the four simulations is also clearly visible in Fig. 6 which shows the time–averaged pressure distribution (C_p) on the plate. For the two–dimensional simulation and for case I ($0.1 \times c$) the vortex on the rear part of the plate leads to a pronounced pressure minimum on the leeward side, which disappears completely when the spanwise extension of the domain is sufficient as shown for cases II and III. Then the pressure in the large recirculation region is nearly constant as expected for a stalled high–lift configuration.

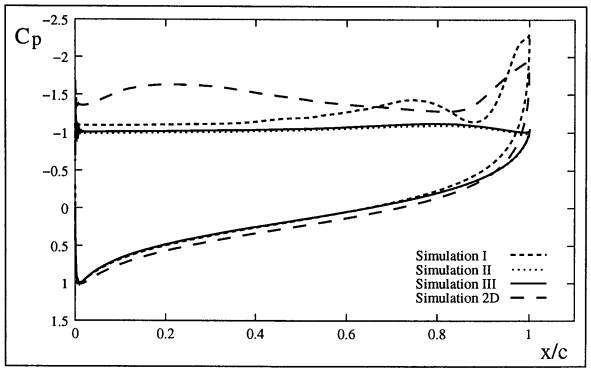

Figure 6: C_p distribution of all simulations.

Furthermore, there are discrepancies in the time–averaged flow structure between the three depicted cases in the vicinity of the leading edge and on the upper surface of the plate. In Fig. 3 for the 2D case a vortex attached to the leading edge of the plate is clearly visible. A tiny vortex also exists rearward the leading edge in the third simulation (III in Fig. 5) but is hardly visible. In simulation I with a spanwise extension of $0.1 \times c$ (see Fig. 4) this leading edge vortex is not existing. Contrary to the other cases, an additional vortex is attached to the surface at about the middle of the plate.

Each of these attached vortices is rotating counterclockwise. The origin of these eddies is given by the interaction of upstream flow induced by the trailing edge vortex and the downstream flow coming from the leading edge. Due to the fact that the trailing edge vortex in case III is shifted somewhat downstream in comparison with the other two cases, it does not induce as much upstream flow and hence the counterclockwise rotating eddy remains smaller.

Table 2 provides a comparison of integral quantities derived from the conducted simulations. The mean lift ($\overline{C}_l$) and drag coefficients ($\overline{C}_d$) are given together with the correspond-

	$\overline{C}_l$	$\overline{C}_d$	$\sigma_{\overline{C}_l}$	$\sigma_{\overline{C}_d}$	St	St'
2D	1.69	0.57	0.622	0.197	0.45	0.139
I	1.32	0.45	0.271	$8.6 \cdot 10^{-2}$	0.53	0.164
II	1.11	0.37	$6.6 \cdot 10^{-2}$	$2.1 \cdot 10^{-2}$	0.63	0.195
III	1.12	0.38	$6.9 \cdot 10^{-2}$	$2.2 \cdot 10^{-2}$	0.66	0.204

Table 2: Comparison of integral quantities.

ing values for the standard deviations ($\sigma_{\overline{C}_l}$, $\sigma_{\overline{C}_d}$). As expected for the two–dimensional case the predicted forces are much too large compared with cases II and III. Furthermore, the variation of the forces ($\sigma_{\overline{C}_l}$, $\sigma_{\overline{C}_d}$) are about one order of magnitude larger than in II and III. In order to understand this phenomenon Fig. 7 depicts the distribution of the instantaneous vorticity ω_z. For comparison a sequence of the three–dimensional case (III) is shown in Fig. 8. Large qualitative discrepancies exists between both cases. In the 2D case the entire flow field is dominated by large vortices generated at the leading and trailing edges. Contrary to simulation III no small–scale vortical structures are present. This is due to the missing vortex stretching and tilting effect in the 2D simulation, a phenomenon which is well known from other flow configurations (Breuer, 1998). However, the main idea behind the 2D simulation was to get affirmed that simulation I tends to a 2D case. Comparing the lift and drag coefficients and their standard deviations in Table 2 it is clearly visible that all quantities of case I are in between the two–dimensional case on the one hand and the cases II and III on the other hand. Simulation I shows three–dimensional effects as seen in cases II and III, but the spanwise domain size is definitely too short and hence suppresses at least partly the development of 3D structures in the wake. Therefore, in contrast to the LESFOIL investigation (Davidson, 2000) the domain size of $0.1 \times c$ is insufficient for the Reynolds number considered in the present study. Additionally, the lift and drag coefficients in simulations II and III do not differ much and thus indicate no need for a further improvement of grid resolution. The Strouhal numbers of the vortex shedding at the trailing edge $St = fc/u_\infty$ (and $St' = fc'/u_\infty$ scaled with the windward width $c' = c \cdot sin\ \alpha$) show the same trend. In conclusion, contrary to the cases 2D and I, simulation III (and II) leads to physically reliable results. Therefore, further discussion is restricted to this configuration.

Discussion of Case III

Fig. 8 depicts the development of the flow field by contour plots of the vorticity component ω_z. Four different phases with a time increment of 0.5 dimensionless time units are shown representing one typical vortex shedding cycle. The corresponding Strouhal number is about $St \approx 0.66$ or $St' \approx 0.2$. These values are consistent with experimental findings which observed a nearly constant $St' \approx 0.15$ for $20° \leq \alpha \leq 90°$ and a strong increase of St' for $\alpha \leq 20°$ (see e.g. Knisely, 1990 and the cited refs.). The two shear layers developing at the leading and trailing edges of the plate, respectively, are of unequal strength. It is found that the counterclockwise vortex generated in the vicinity of the trailing edge is dominating the entire wake of the inclined plate. During its initial phase (a–b) this vortex is attached to the trailing edge of the plate while vorticity is accumulated in it being fed by the corresponding shear layer. The size of this vortex is continuously increasing. After it has reached a diameter of about $0.25c$ (c), the vortex is shed and convected downstream, while diffusion of vorticity takes place. Then a new shedding cycle begins (d).

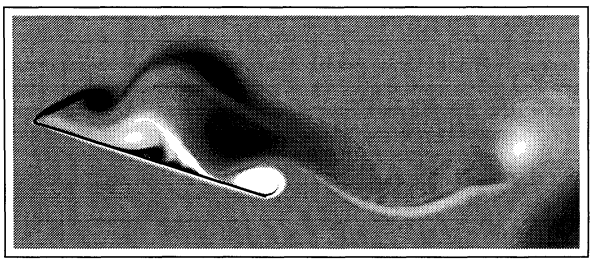

Figure 7: Instantaneous vorticity ω_z, Simulation 2D.

Behind the leading edge a Kelvin–Helmholtz instability is detected in the free shear layer. Furthermore, fluid circulation in clockwise direction is observed leading to a large recirculation region on the leeward side of the flat plate. As already shown in Fig. 6, a nearly constant pressure distribution is found in the separation region on the leeward side of the plate. However, no regular shedding motion of vortices generated at the leading edge is visible. The size of the attached clockwise rotating recirculation region is strongly depending on the presence, the size and the strength of the counterclockwise vortex structure arising at the trailing edge. While the counterclockwise vortex is increasing in size and strength, the region of clockwise rotating fluid is decreasing. However, after the trailing edge vortex is shed from the plate edge and convected downstream, the clockwise vortex has enough space to extend in size until the next trailing edge vortex is developing. In contrast to classical

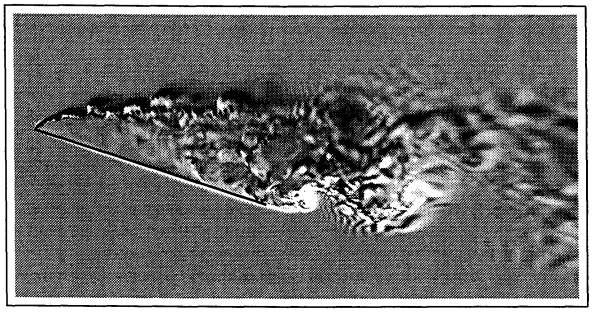

(a) T_0

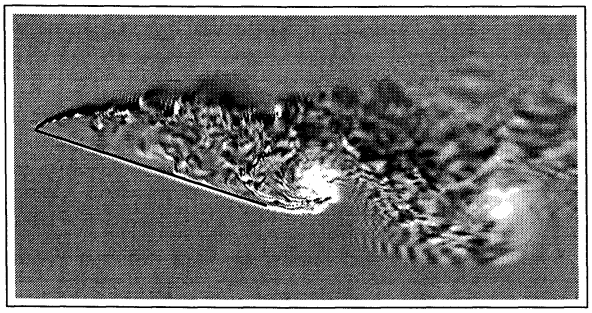

(b) $T_0 + 0.5$

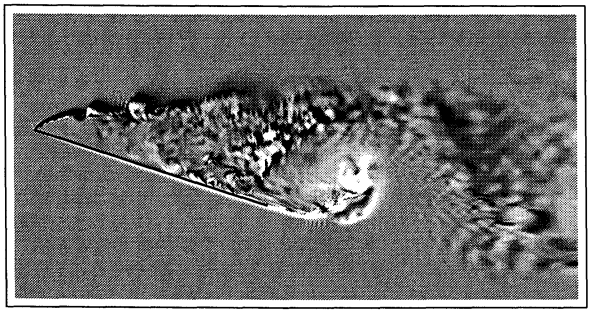

(c) $T_0 + 1.0$

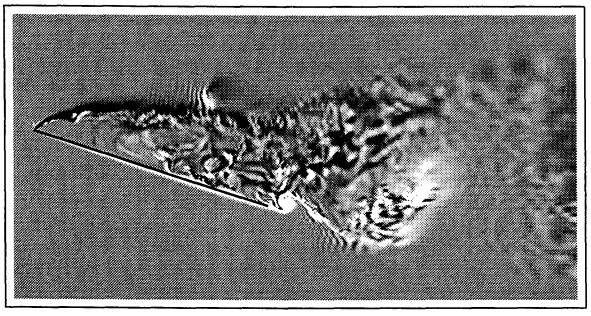

(d) $T_0 + 1.5$

Figure 8: Vortex shedding cycle past the inclined flat plate at $\alpha = 18°$ and $Re_c = 20,000$, contours of vorticity ω_z at four different phases.

vortex shedding past circular cylinders or normal flat plates showing well–established staggered arrangements of vortices of opposite sign and equal strength, for the flow past the inclined flat plate at an angle of attack in the range investigated a highly asymmetric wake with vortices of unequal strength is observed (see Fig. 9). These observations are in close agreement with experimental findings for an inclined plate by Lam (1996) [$\alpha = 30°$, $Re_c = 30,000$], Perry and Steiner (1987) [$\alpha = 45°$, $Re_c = 20,000$] and Knisely (1990). A three–dimensional visualization of the flow field by iso–surfaces of the instantaneous pressure is given by Fig. 10. It clearly shows large scale vortical structures in the wake as well as the breakup of shear layers into smaller structures behind the leading and trailing edge.

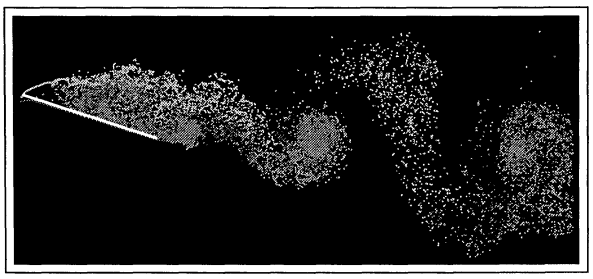

Figure 9: Visualization of the asymmetric vortex street behind the inclined flat plate, $\alpha = 18°$, $Re_c = 20,000$.

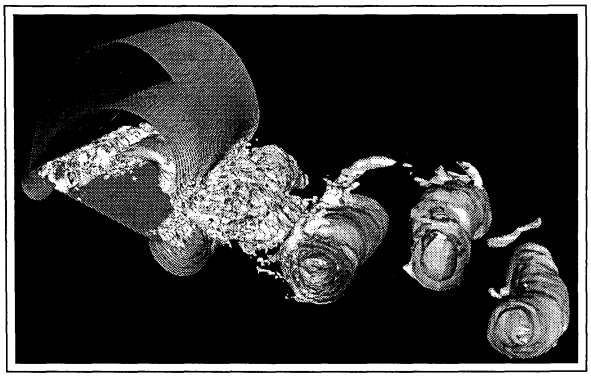

Figure 10: Iso–surfaces of the pressure for the inclined flat plate, $\alpha = 18°$, $Re_c = 20,000$.

Additionally, Fig. 11 depicts the distribution of the total resolved Reynolds stresses $\overline{u'u'}$, $\overline{v'v'}$, and $\overline{u'v'}$, respectively. These components include the periodic and the turbulent fluctuations. In order to separate both components, phase–averaging has to be carried out which is associated with several difficulties due to slightly varying shedding periods and therefore omitted here. As expected, the largest values especially of $\overline{v'v'}$ are found in the vicinity of the trailing edge mainly caused by the quasi–periodic shedding motion of the trailing vortex. In the entire low–pressure recirculation region the Reynolds stresses are very low with the exception of the shear layer region where the Kelvin–Helmholtz instability is observed. These plots strongly support the finding, that the asymmetric vortex structure past the inclined plate is dominated by the shedding mechanism at the trailing edge.

CONCLUSION

In the present investigation the separated flow past an inclined plate was investigated

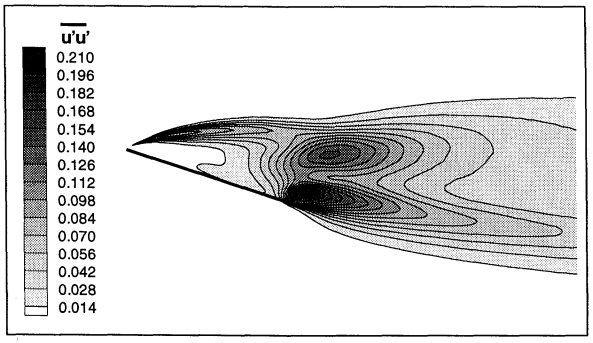

(a) $\overline{u'u'}$

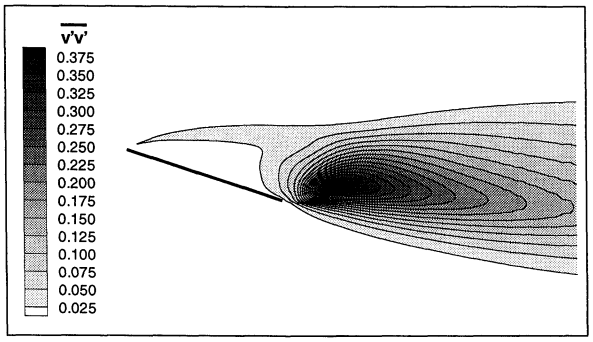

(b) $\overline{v'v'}$

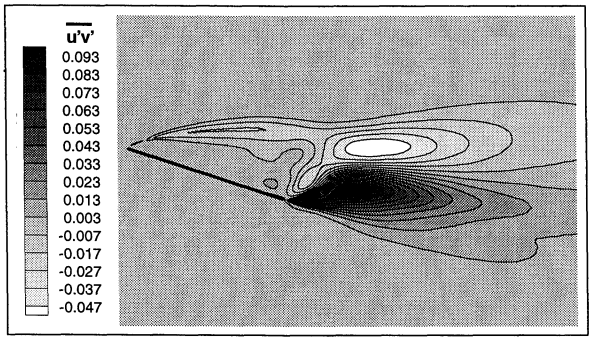

(c) $\overline{u'v'}$

Figure 11: Resolved Reynolds stresses for the flow past the inclined flat plate, $\alpha = 18°, Re_c = 20,000$.

by LES, which is an appropriate tool for flows with large–scale vortical structures and recirculation regions. The flow in the wake of the plate is definitely three–dimensional. If this degree of freedom is suppressed in the simulation either by restriction to a two–dimensional simulation or by a too narrow integration domain in spanwise direction, totally different flow structures appear. After this evaluation procedure the final configuration was studied in detail. These LES results show that the entire flow field is strongly dominated by the development and shedding behavior of the trailing edge vortex. First results of the flow around the NACA–4415 profile at the same flow conditions indicate very similar flow features as observed for the inclined plate. Owing to the knowledge of the dominating trailing edge vortex for the plate, this observation is not astonishing. In both cases the geometry of the trailing edge is only slightly different leading to comparable trailing edge vortices. The airfoil case is the subject of ongoing research.

REFERENCES

Breuer, M., Rodi, W., 1996, "Large–Eddy Simulation of Complex Turbulent Flows of Practical Interest", In: *Flow Simulation with High–Performance Computers II*, ed. E.H. Hirschel, *Notes on Numerical Fluid Mechanics*, Vol. 52, pp. 258–274, Vieweg Verlag, Braunschweig.

Breuer, M., 1998, "Large Eddy Simulation of the Sub–Critical Flow Past a Circular Cylinder: Numerical and Modeling Aspects", *Int. J. for Numerical Methods in Fluids*, Vol. 28, pp. 1281–1302, J. Wiley & Sons Ltd, Chichester.

Breuer, M., 2000, "A Challenging Test Case for Large Eddy Simulation: High Reynolds Number Circular Cylinder Flow", *Int. J. of Heat and Fluid Flow*, Vol. 21, no. 5, pp. 648–654, Elsevier Science B.V., Amsterdam.

Davidson, L., 2000, "LESFOIL: An European Project on Large Eddy Simulations Around a High–Lift Airfoil at High Reynolds Number", in: *ECCOMAS 2000, European Congress on Computational Methods in Applied Sciences and Engineering*, 11–14 Sept. 2000, Barcelona, Spain.

Knisely, C.W., 1990, "Strouhal Numbers of Rectangular Cylinders at Incidence: A Review and New Data", *J. of Fluids and Structures*, Vol. 4, pp. 371–393.

Lam, K.M., 1996, "Phase–Locked Eduction of Vortex Shedding in Flow Past an Inclined Flat Plate", *Physics of Fluids*, Vol. 8 (5), pp. 1159–1168.

Lerche, Th., Dallmann, U. Ch., 1999, "Das Prinzipexperiment COSTWING I: Dokumentation der Aufbauphase", Inst. f. Strömungsmechanik, DLR Göttingen, IB 223–99 A04.

Perry A.E., Steiner, T.R., 1987, "Large–Scale Vortex Structures in Turbulent Wakes Behind Bluff Bodies, Part 1: Vortex Formation Process", *J. of Fluid Mechanics*, Vol. 174, pp. 233–270.

Rodi, W., Ferziger, J.H., Breuer, M., Pourquié, M., 1997, "Status of Large Eddy Simulation: Results of a Workshop", *Workshop on LES of Flows past Bluff Bodies*, Rottach–Egern, Tegernsee, Germany, June 26–28, 1995, *J. of Fluids Engineering*, Vol. 119, no. 2, pp. 248–262.